Nanoscale

Accepted Manuscript

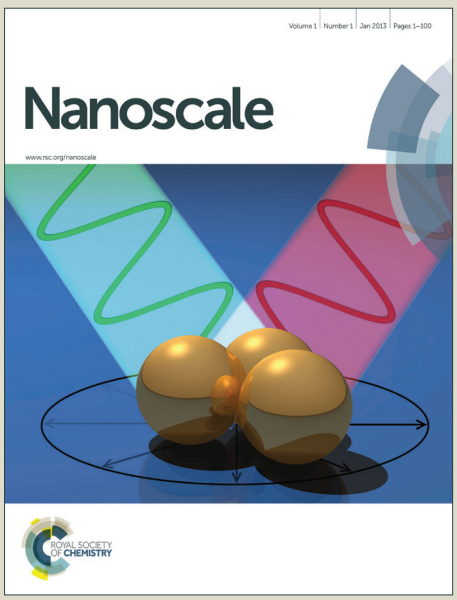

ROYAL SOCIETY OF CHEMISTRY

www.rsc.org/nanoscale

Nanoscale

Dynamic Article Links ►

Cite this: DOI: 10.1039/c0xx00000x

www.rsc.org/nanoscale

PAPER

Controlled Synthesis, Asymmetrical Transport Behavior and Luminescence Properties of Lanthanide Doped ZnO Mushroom-like 3D Hierarchical Structures

Dan Yue,‡[a, b] Wei Lu,‡[c] Lin Jin,[a] Chunyang Li,[a] Wen Luo,[a] Mengnan Wang,[a] Zhenling Wang*[, a] and Jianhua Hao*[, c]

Received (in XXX, XXX) Xth XXXXXXXXX 20XX, Accepted Xth XXXXXXXXX 20XX

DOI: 10.1039/b000000x

Lanthanide doped ZnO mushroom-like 3D hierarchical structures have been fabricated by polyol-mediated method and characterized by various microstructural and optical techniques. The results indicate that the as-prepared ZnO: Ln^{3+} (Ln = Tb, Eu) samples have hexagonal phase structure and possess mushroom-like 3D hierarchical morphology. The length of the whole mushroom from stipe bottom to pileus top is about 1.0 μm, and the diameters of pileus and stipe are about 0.8 μm and 0.4 μm, respectively. It is found that the flow of N_2 atmosphere is the key parameter for the formation of the novel ZnO structure and the addition of $(NH_4)_2HPO_4$ has a prominent effect on the phase structure and the growth of mushroom-like morphology. The potential mechanism of forming this morphology is proposed. The pileus of the formed mushroom is assembled by a number of radial ZnO: Ln^{3+} nanorods, while the stipe is composed of over layered ZnO: Ln^{3+} nanosheets. Moreover, asymmetrical *I–V* characteristic curves of ZnO: Ln^{3+} mushrooms indicate that the texture composition of the 3D hierarchical morphology might lead to the asymmetrical transport behavior of electrical conductivity. Lanthanide doped ZnO samples can exhibit red or green emission under the excitation of UV light.

1. Introduction

As an important II–VI group semiconductor, zinc oxide (ZnO) has extensive applications in many fields, such as optoelectronic devices, photocatalyst, cell and piezoelectric power generator because of its intrinsic features, including direct band gap (*E*g=3.37 eV) and large exciton binding energy (60 meV).[1] The unique optical, acoustic and electronic properties of ZnO as well as the morphology control have been studied by many researchers in the last decades.[2a,b] Recently, vanadium (V)-doped two-dimensional ZnO nanostructures, ZnO hybrid nanostructures on graphere and ZnO nanosheets/anionic layer heterojunction were prepared, showing potential application for high-performance flexible direct current (DC) power piezoelectric nanogenerators.[2c-e] It is known that the functional properties of the obtained materials are lain on their structural and morphological characteristic. The plenty of previous literatures have confirmed that ZnO probably exhibits the most splendid family of nanostructure morphologies, such as nanowires, nanotubes, nanobelts, nanosprings, nanohelices, rod-needle nanostructures, etc.[3]

Construction of nanostructures of complex morphologies, hierarchical architecture and orientation is one of the challenging tasks in material science field.[1e, 4] The purposeful synthesis of ZnO with particular morphology, understanding the growth mechanism of different morphologies and thus realizing to controll the morphology are very interesting not only in basic study but also in practical applications. Wang et al. and other groups have done many original contributions to enrich the morphology of ZnO, explore the synthesis techniques and develop their use in some new fields. For example, nanospring, nanorings and helical nanostructures are formed by rolling up free-standing ZnO nanobelt,[3b, 5] and single-crystal hexagonal ZnO disks can also be converted into rings by controlling growth temperature and molar ratio of reactants.[6] Horizontally aligned ZnO nanowires with full control over the width and length have been fabricated by a wet chemical method, which are promising in optical gratings, integrated circuit interconnects and light-emitting diodes.[7] Wu et al. reported that the vertically aligned ZnO nanorod arrays could be epitaxially grown on various substrates, such as Zn sheets, Si wafers and transparent glass.[4c] Hierarchical structure such as tree- and cockscomb-like ZnO arrays have been grown *in situ* on zinc plates through a simple hydrothermal oxidation approach, and these morphologies can be controlled by the addition of co-solvent ethylenediamine (en).[8] ZnO twin-spheres have been successfully produced through stepwise self-assembly growth and exhibited anisotropic blue emission.[9] Some special morphologies such as mushroom-like and cauliflower-like ZnO microcrystals and their photocatalytic activities have been reported by a few literatures.[10]

Though ZnO exhibits several kinds of morphologies, the controllable synthesis of lanthanide doped ZnO mushroom-like (very similar to wild lentinus edodes) 3D hierarchical and asymmetrical structures has been rarely reported. Furthermore, the formation mechanism and affecting factors leading to this morphology are still unclear. Mushroom-like morphology is a typical asymmetrical structure and such system is valuable in the creation of complex structures through anisotropic interactions. Compared with other morphologies, particles with mushroom-like morphology might have some potential applications in photonics and other fields.[11] For example, it has been confirmed that some materials (Janus polymer, TiO_2) with this morphology might have some unique structural characteristic and pH-responsive property.[11] Moreover, lanthanide ions with rich energy levels can be doped into ZnO crystal lattice, which makes these materials have unique optical properties and promising applications in optoelectronic devices.[12] Herein, we report a mushroom-like 3D hierarchical morphology formed by self-assembly of ZnO: Ln^{3+} nanostructures in a polyol-mediated solution which was used to synthsize $LaPO_4$,[13] Ag nanocubes,[14] fluorides[15] and so on. It is found that the addition of

$(NH_4)_2HPO_4$ and bubbling of N_2 atmosphere in the reaction solution are the two key factors for the formation of muchroom-like morphology. The formation mechanism of mushroom-like 3D hierarchical morphology was proposed based on the analysis of XRD, SEM and TEM. Furthermore, *I–V* characteristics of ZnO: Ln^{3+} mushrooms were investigated by *in situ* TEM technique and exhibit asymmetrical transport behavior. These mushroom-like ZnO: Ln^{3+} (Ln = Tb, Eu) show the characteristic green and red emission for Tb^{3+} and Eu^{3+} ions, respectively. Our results make these materials be attractive in the potential fields, such as fluorescent lamps, field emission displays, photocatalysis, sensors, etc.

2. Results and Discussion

2.1. Morphology and Structure of ZnO: Ln^{3+} Mushrooms

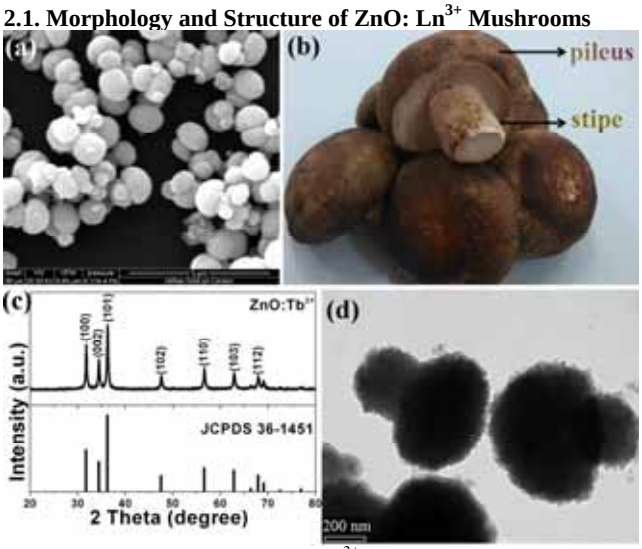

Fig. 1 (a) SEM image of ZnO: Tb^{3+} mushrooms, (b) photograph of natural lentinus edodes for comparison, (c) XRD pattern and (d) low-magnification TEM image of ZnO: Tb^{3+} mushrooms.

The morphology and phase structure of ZnO: Tb^{3+} mushrooms were investigated by SEM, TEM and XRD. Fig. 1a gives a SEM image of ZnO: Tb^{3+} sample, which exhibits a typical morphology of mushroom-like ZnO: Tb^{3+}. The asymmetrical mushroom-like morphology is composed of two parts, i.e. pileus and stipe, which is very similar to the natural lentinus edodes (Fig. 1b). The height of the whole mushroom from stipe bottom to pileus top is about 1.0 μm, and the diameters of pileus and stipe are about 800 nm and 400 nm, respectively. The XRD patterns of ZnO: Tb^{3+} mushrooms (Fig. 1c) show that all of the diffraction peaks are in agreement with the standard data of bulk ZnO (JCPDS card, No. 36-1451) and can be identified as hexagonal structured ZnO with space group of $P6_3mc$. No peaks of any other phases or impurities are detected, indicating the high purity of these samples. The strong and sharp diffraction peaks also confirm the good crystallization of the ZnO: Tb^{3+} mushrooms. The mushroom-like morphology could be clearly observed from the low-magnification TEM image shown in Fig. 1d. There are a large number of nanocrystals at the edge of the ZnO: Tb^{3+} mushrooms, indicating that the mushroom-like 3D hierarchical structures might be assembled by many primary nano-units through some specific assembly way.

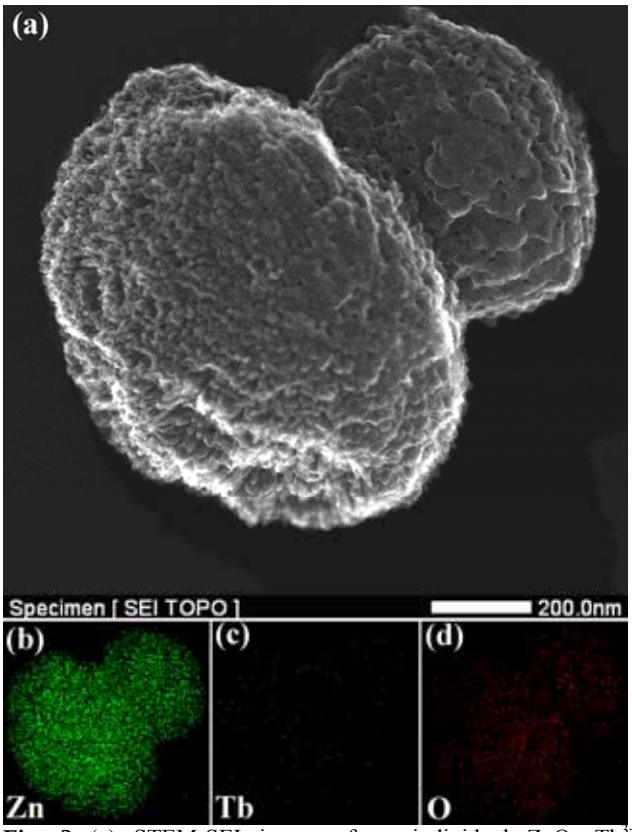

Fig. 2 (a) STEM-SEI image of an individual ZnO: Tb^{3+} mushroom. (b)~(d) EDS elemental mapping images for Zn, Tb and O of the individual mushroom shown in (a), respectively.

Fig. 2a shows the morphology of an individual ZnO: Tb^{3+} mushroom acquired in STEM-SEI (secondary electron imaging) topology mode, through which the 3D hierarchical and asymmetrical mushroom can be observed, thus the assembly manner of the pileus and stipe can be deduced based on the microstructural analysis. It can be seen from Fig.2a that the surface of the pileus (head area) is composed of many nanoparticles which is actually the tip end of many nanorods, which can also be confirmed by high resolution electron microscopy in the following paragraph. The observation indicates that the pileus area of mushroom-like morphology is radially assembled by lots of ZnO: Tb^{3+} nanorods. However, the growth behavior of stipe (root area) of the mushroom is not similar to that of the pileus, and the stipe is composed of many ZnO: Tb^{3+} nanosheets which is formed by the layer-by-layer superposition. The EDS element mappings of Zn (Fig. 2b), Tb (Fig. 2c) and O (Fig. 2d) elements show that the mushroom is composed of even Zn and O elements with doped Tb randomly. As for ZnO: Eu^{3+}, the morphology is still mushroom-like 3D hierarchical structure. This indicates that the replacement of Tb ions by doping Eu ions has little effect on the mushroom morphology. The EDS element mappings of Zn, Eu and O elements are shown in Fig. S1, which indicates that the doping Eu ions can be dispersedly distributed into the mushroom-like 3D hierarchical structure.

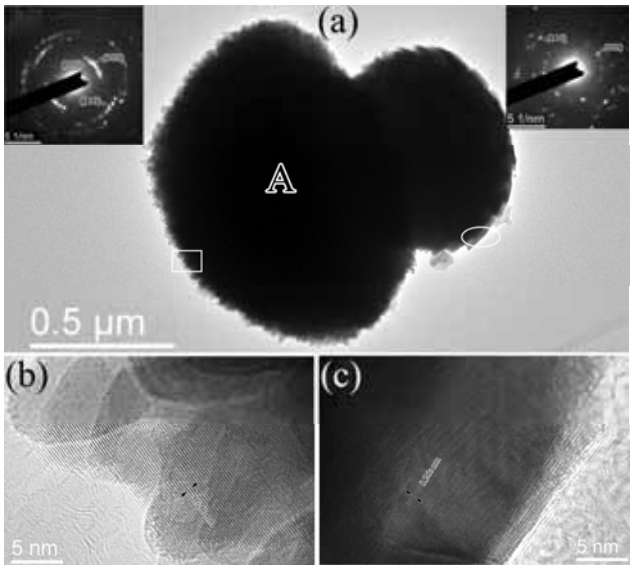

Fig. 3 TEM images of a typical ZnO: Tb^{3+} mushroom. (a) The BF image of the mushroom and the corresponding electron diffraction patterns (the left inset is from the pileus area, and the right inset is from the stipe area), and HRTEM images of the area indicated by (b) white rectangular and (c) white oval in (a).

To investigate the growth behavior of this morphology in detail, the microstructure of ZnO: Tb^{3+}mushrooms was analyzed by TEM-bright field (BF), high-resolution transmission electron microscopy (HRTEM) images and selected area electron diffraction (SAED) patterns. The BF image of a typical ZnO mushroom (Fig. 3a) shows that it is composed of pileus and stipe. The SAED pattern in the left inset taken from the pileus area is different from that in right inset from the stipe area. Firstly, the first order of diffraction patterns has a shape of arc in the left inset, while it has a round shape with scattered spots in the right inset. Secondly, the first order of diffraction patterns is broadening along radial direction in the left inset. However, it has sharp spots in the right inset. The diffraction patterns with an arc shape in the left inset mean that the head of the mushroom has a textured composition,[16] also indicating the formation of pileus from the radially assemble of ZnO: Tb^{3+} nanorods. The broadening strong arc in the left inset can be indexed as the mixed planes of $(100)_{ZnO}$ and $(002)_{ZnO}$. The plane distance difference between $(100)_{ZnO}$ and $(200)_{ZnO}$ is only 0.022 nm, thus they will mix together in the first order of diffraction pattern which leads to the broadening along radial direction. According to HRTEM image in Fig. 3b, it can be seen that the pileus part is composed of ZnO nanorods growth along c direction. The HRTEM image of stipe part in Fig. 3c shows that this part is composed of nanosheets growth along c direction. Therefore, it is interesting to consider why $(100)_{ZnO}$ diffraction patterns can be gotten in the pileus area while disappeared in the stipe area. The possible mechanism behind the observation is related to the three-dimensional morphology of ZnO mushroom. The pileus area is composed by ZnO nanorods with radial morphology, and in the center area of "A" as denoted in Fig. 3a, there are some ZnO rods whose c direction is parallel with electron beam. Hence, the $(100)_{ZnO}$ planes can be seen in the diffraction pattern. Meanwhile, the stipe area is composed of ZnO nanosheets assembled by the layer-by-layer superposition. The c direction of sheets will be perpendicular to electron beam, hence the $(100)_{ZnO}$ planes will disappear in the diffraction patterns.

2.2. The Controlled Synthesis of ZnO: Ln^{3+} Mushrooms

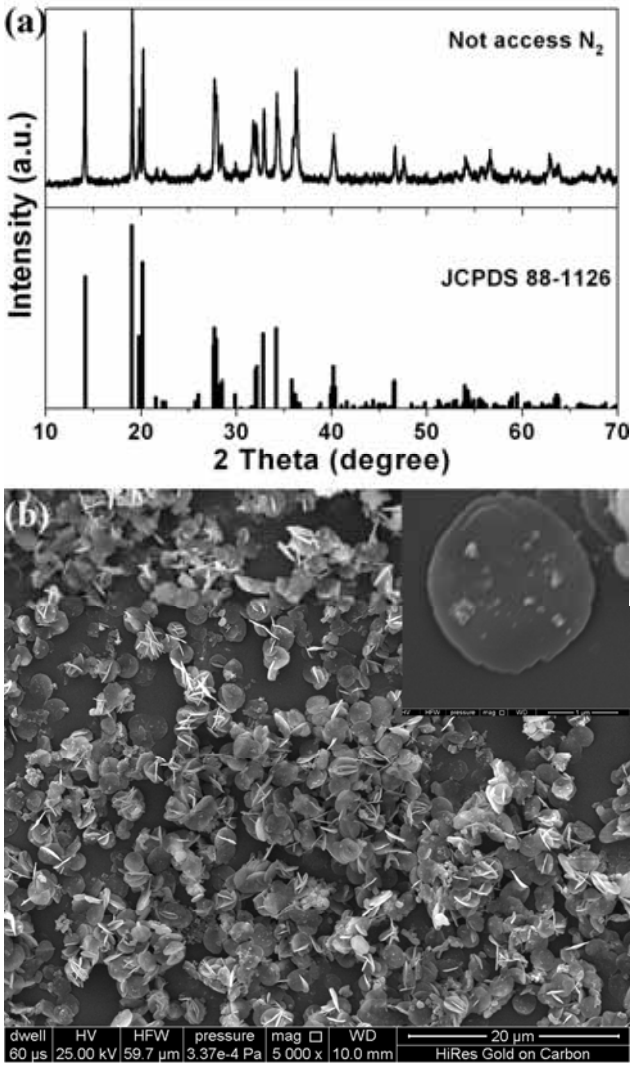

Fig. 4 (a) XRD patterns of sample without bubbling N_2 and (b) SEM images of NH_4ZnPO_4 nanowafers. (Inset is the high-magnification images of a nanowafer).

Regarding to the formation of the specific morphology, one of the key factors is bubbling of N_2 atmosphere for the phase formation of ZnO: Ln^{3+} mushrooms. When a flow of N_2 atmosphere was not bubbled into the reaction system, it can be seen from the XRD result that ZnO: Ln^{3+} cannot be obtained. The diffraction peaks of the obtained sample can be identified as monoclinic structures with the space groups of P_{21}, agreeing with the standard data of bulk NH_4ZnPO_4 (JCPDS No. 88-1126), as shown in Fig. 4a. The SEM images (Fig. 4b) indicate that the morphology of NH_4ZnPO_4: Ln^{3+} is composed of nanowafer with an average diameter of 2.2 μm and thickness of about 90 nm. The $(NH_4)_2HPO_4$ added into the reaction system can be decomposed into NH_3, H^+ and PO_4^{3-} at high temperature. Without bubbling of N_2 atmosphere, NH_3 bubbles are not easy to escape from the solution because of the high surface tension of minute bubbles with a small radius of curvature and the high solubility in water solution. Therefore, NH_3 will be reacted with H^+ to form NH_4^+ cations in reaction solution, thus NH_4ZnPO_4 is formed as given in reaction equation (1).

$$Zn^{2+} + NH_4^+ + PO_4^{3-} \xrightarrow{heat} NH_4ZnPO_4\ (s) \qquad (1)$$

When a flow of N_2 atmosphere was bubbled into the reaction system, N_2 bubbles make the primary curvature radius of NH_3

minute bubbles enlarge which leads to the low surface tension, thus NH_3 bubbles could be easily generated and were captured out of the reaction solution by the flow of N_2 bubbles. The addition of $(NH_4)_2HPO_4$ at a relatively low concentration might not affect the phase structure of ZnO, instead control the mushroom morphology of the as-prepared samples.

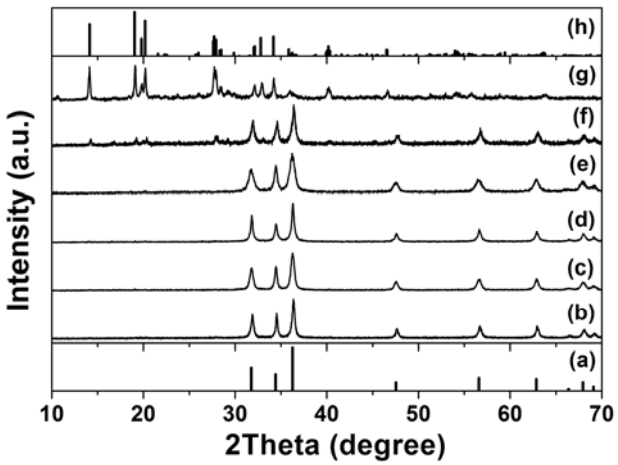

Fig. 5 XRD patterns of samples with different amounts of $(NH_4)_2HPO_4$: (a) the standard data of hexagonal ZnO powders (JCPDS No. 36-1451), (b) 0 mmol, (c) 0.95 mmol, (d) 4.75 mmol, (e) 9.5 mmol, (f) 19.0 mmol, (g) 95.0 mmol, and (h) the standard data of orthorhombic NH_4ZnPO_4 powders (JCPDS No. 88-1126).

In order to further understand the controlled synthesis of the ZnO: Ln^{3+} mushrooms, the effect of different amounts of $(NH_4)_2HPO_4$ on the phase structure and morphology of the obtianed samples was also investigated systematically. Fig. 5 shows the XRD patterns of the samples prepared under a flow of N_2 atmosphere with the addition of different amounts of $(NH_4)_2HPO_4$. When the amount of $(NH_4)_2HPO_4$ changes from 0 to 9.5 mmol (Fig. 5b~e), the samples have similar XRD patterns in profile, and all diffraction peaks can be indexed to hexagonal structured ZnO (JCPDS No. 36-1451). When $(NH_4)_2HPO_4$ was not added into this reaction system, the water of crystallization in $Zn(CH_3COO)_2{\cdot}2H_2O$ could be removed and $Zn(CH_3COO)_2$ could be decomposed into ZnO particles at the reaction temperature of 160 °C. The possible formation mechanism of ZnO is described as a series of equations (2~5):[17]

$$Zn(CH_3COO)_2{\cdot}2H_2O \xrightarrow{heat} Zn(CH_3COO)_2 + 2H_2O \quad (2)$$

$$4Zn(CH_3COO)_2 + H_2O \xrightarrow{heat} Zn_4O(CH_3COO)_6 + 2CH_3COOH\uparrow \quad (3)$$

$$Zn_4O(CH_3COO)_6 + 3H_2O \xrightarrow{heat} 4ZnO\ (s) + 6CH_3COOH\uparrow \quad (4)$$

$$Zn_4O\ (CH_3COO)_6 \xrightarrow{heat} 4ZnO\ (s) + 3CH_3COCH_3\uparrow + 3CO_2\uparrow \quad (5)$$

It is easy for the $(NH_4)_2HPO_4$ added into the reaction system to decompose under high temperature, therefore NH_3 gas began to appear when the reaction temperature was increased up to approximate 160°C. When the amount of $(NH_4)_2HPO_4$ is relatively low (0.95~9.5 mmol), one part of NH_3 gas is captured out of the reaction solution by the flow of N_2 bubbles, and the other small part of NH_3 gas is dissolved into the solution. Hence, the solution will become alkaline condition and then the Zn^{2+} ion could react with NH_3 molecules to form $Zn(NH_3)_4^{2+}$ complex. Accordingly, the reaction for forming ZnO can be expressed as the reaction equation (2~5) or (6~7).

$$Zn^{2+} + 4NH_3 \longrightarrow Zn(NH_3)_4^{2+} \quad (6)$$

$$Zn(NH_3)_4^{2+} + 2OH^- \longrightarrow ZnO\ (s) + 4NH_3 + H_2O \quad (7)$$

With gradually increasing the amount of $(NH_4)_2HPO_4$ to 19.0 mmol, the amount of NH_3 gas dissolved into the solution will be increased and more and more NH_3 will be reacted with H^+ to form NH_4^+ cations in reaction solution. The increasing of the concentration of NH_4^+ cations and PO_4^{3-} anions leads to the formation of NH_4ZnPO_4 with monoclinic phase (JCPDS No. 88-1126),[18] and then the mixture of ZnO and NH_4ZnPO_4 is obtained, as shown in Fig. 5f. With further increasing the amount of $(NH_4)_2HPO_4$ to 95.0 mmol, the concentration of NH_4^+ cations and PO_4^{3-} anions in solution should be sufficiently increased to obtain the pure monoclinic phase NH_4ZnPO_4,[18] as given in Eq. 1 and Fig. 5g.

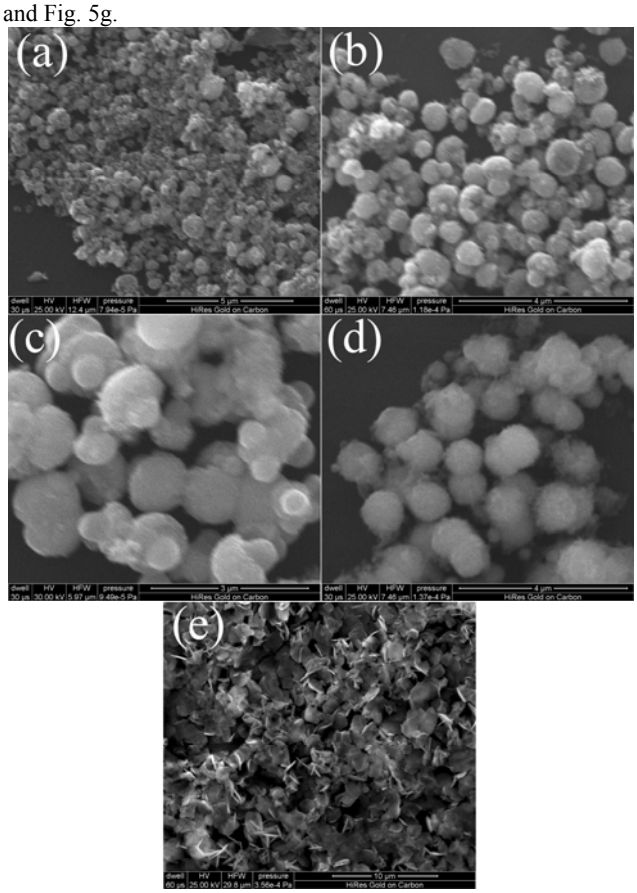

Fig. 6 SEM images of samples synthesized from different amounts of $(NH_4)_2HPO_4$: (a) 0 mmol, (b) 0.95 mmol, (c) 4.75 mmol, (d) 19.0 mmol and (e) 95.0 mmol.

It is found that the addition of $(NH_4)_2HPO_4$ is another important controlling factor not only in the course of phase transformation from ZnO to NH_4ZnPO_4, but also in the formation process of mushroom-like morphology. Fig. 6a presents the SEM image of the sample synthesized without the addition of $(NH_4)_2HPO_4$, from which we can see that ZnO is composed of irregular nanoparticles. When 0.95 mmol of $(NH_4)_2HPO_4$ was added, its morphology was mainly composed of irregular nanoparticles and the mushroom-like morphology began to appear, as shown in Fig. 6b. With gradually increasing the amount of $(NH_4)_2HPO_4$ to 4.75 mmol, it can be clearly observed from Fig. 6c that the mushroom-like morphology was formed, and the length of mushrooms varies from 1.0 ~ 1.2 μm, the pileus diameter is about 0.8 ~ 1.0 μm and the stipe is about 0.40 μm. Fig. 6d gives SEM image of the sample obtained by adding 19.0

mmol of $(NH_4)_2HPO_4$, and it shows that the sample mainly consists of sphere-like structures with the diameter of approximately 0.88 μm. If the amount of $(NH_4)_2HPO_4$ was further increased to 95.0 mmol, the pure monoclinic NH_4ZnPO_4 was formed according to the result of XRD, and the sample was composed of nanosheet-like structures, as shown in Fig. 6e.

2.3. The Formation Mechanism of ZnO: Ln^{3+} Mushrooms

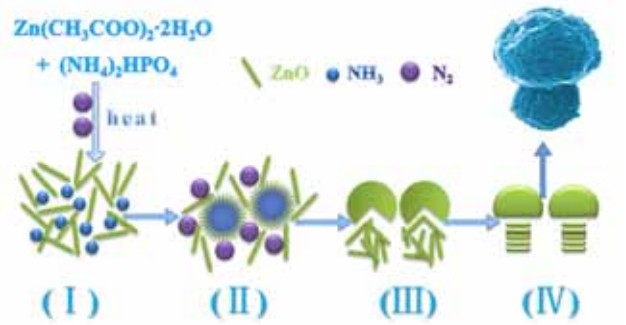

Scheme 1. Schematic illustration of the evolution process of obtained ZnO: Ln^{3+} mushrooms.

As mentioned above, the bubbling of N_2 atmosphere and the addition of a desired amount of $(NH_4)_2HPO_4$ are the two dominating factors in the phase formation and mushroom-like morphology growth of ZnO: Ln^{3+}. A schematic illustration of Scheme 1 shows the evolution process of ZnO: Ln^{3+} mushrooms. In the first stage (I), $Zn(CH_3COO)_2{\cdot}2H_2O$ dissolved in reaction solution was decomposed by heating to form many primary ZnO nanostructures (nanorods, nanosheets) under the existence of N_2 bubbles and $(NH_4)_2HPO_4$. In the following anisotropic growth stage (II), the random nanorods first gathered around the bubbles and aggregated into many spheres via Ostwald ripening, and then more and more nanorods scatteringly assembled around these spheres. It is known that the density of NH_3 in the standard condition is 0.771 g/L, which is smaller than that of N_2 (1.251 g/L). When the amount of $(NH_4)_2HPO_4$ is appropriate such as 9.5 mmol, there might exist a balance between NH_3 bubbles and N_2 flow in this system. The coexistence of NH_3 and N_2 bubbles and the balance between these two atmospheres might be benefit to form the mushroom-like morphology. In the (III) stage, with the increase of reaction, bubbles will gradually become larger and be fractured, and the spheres assembled by many nanorods will appear gap, thus the pileus of mushroom might be formed. At the same time, many nanosheets probably assembled in parallel by lots of nanorods would be gathered around the gap and stacked through layer by layer to form mushroom stipes. In the (IV) stage, the pileus are combined with stipes to form the ZnO: Ln^{3+} mushrooms.

2.4. *I–V* Characteristics of ZnO: Ln^{3+} Mushrooms

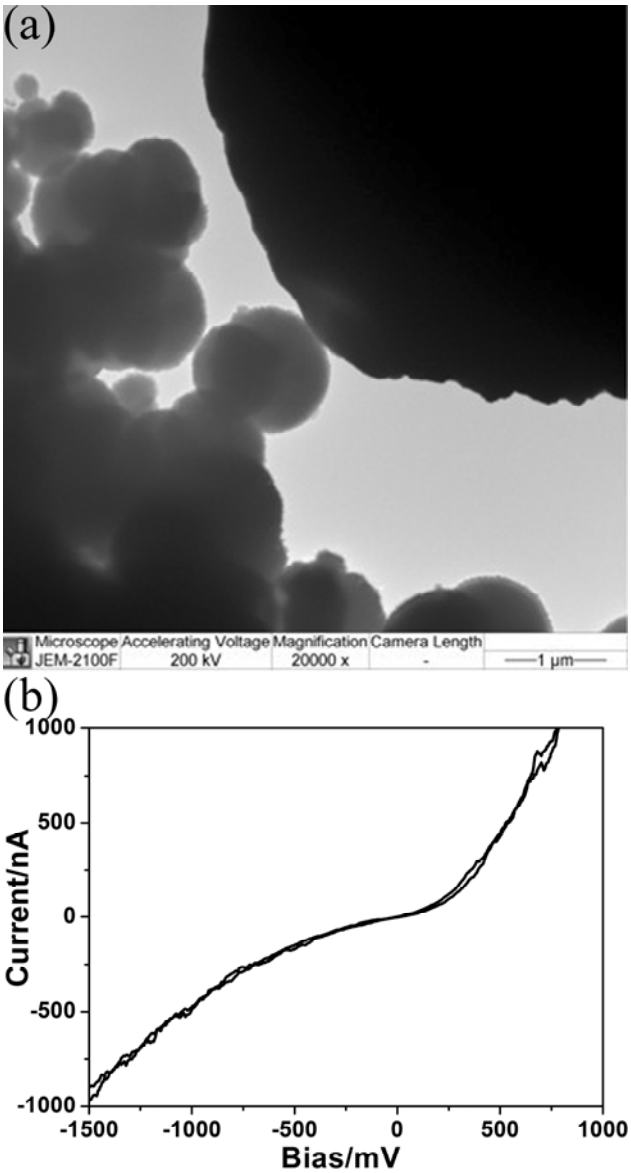

Fig. 7 (a) *In-situ* TEM image and (b) *I–V* characteristics curves of an individual ZnO: Tb^{3+} mushroom.

Fig. 7a shows a circuit curve obtained by *in situ* TEM study. The right up conner is the end of fixed Pt wire connected with one ZnO: Tb^{3+} mushroom. The left down conner is the end of movable Au wire, and the single ZnO: Tb^{3+} mushroom was adhered onto the end of Au wire. Fig. 7b shows the corresponding *I–V* curves of the ZnO: Tb^{3+} mushroom, obtained by sweeping a dual slope of the applied voltage from −1.5 to +1.5 V and then reverse. Firstly, it shows that the loop of the curve is consistent for the dual slope voltage. It shows a typical *I–V* curve in the smaller voltage range (from −1.5 to 0.8 V). This *I–V* curve shows almost linear relationship within 250 mV, and subsequently changes by nonlinear trend when the voltage is greater than 250 mV, implying the decrease in the resistance of ZnO mushrooms. However, the electric current of the forward voltage is higher than that of the reverse voltage. Note that the current is saturated when the bias voltage is increased up to about 0.8 V, meanwhile it is still not saturated when the reverse bias voltage is reached up to -1.5 V. The observed phenomena are associated with the texture composition leading to the anisotropy of electron conductivity.[19]

2.5. Luminescence Properties of ZnO: Ln^{3+} Mushroom

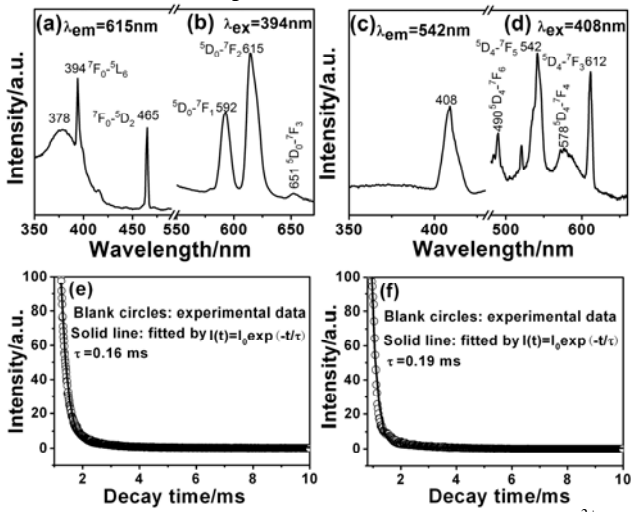

Fig. 8 PL excitation and emission spectra of (a, b) ZnO: Eu^{3+} and (c, d) ZnO: Tb^{3+} mushrooms, and the luminescent decay curves of (e) ZnO: Eu^{3+} and (f) ZnO: Tb^{3+} mushrooms.

Eu^{3+} ions are usually employed as probe to decipher the coordination environment around the substituted cations in the crystalline lattice because the optical transitions of Eu^{3+} are sensitive to their local coordination and thus the emission intensity strongly depends on the crystal structure and crystal-field surrounding around Eu^{3+}.[20] Fig. 8a shows the excitation spectrum of as-obtained ZnO: Eu^{3+} mushrooms monitored at 615 nm emission of Eu^{3+} ions. The broad band at 378 nm is attributed to the transition from valence band to conduction band (VB→CB) of ZnO mushrooms,[21a] and the two peaks at 394 and 465 nm are assigned to $^7F_0 \rightarrow {}^5L_6$ and $^7F_0 \rightarrow {}^5D_2$ transitions of Eu^{3+} ions, respectively.[21b] The emission spectrum (Fig. 8b) is composed of $^5D_0 \rightarrow {}^7F_J$ (J = 1, 2, 3) emission lines of Eu^{3+} ions from 500 to 670 nm.[21b] The analysis of PL spectra indicates that the energy transfer from the ZnO host to Eu^{3+} ions occurred and the doping Eu^{3+} ions could be effectively introduced into the lattices of ZnO mushrooms.[22] It should be denoted that the exact amount of Eu^{3+} ions introduced into the lattices of ZnO is not easy to determined, though the EDS element mappings gave the evidence that the doping Ln^{3+} ions can be dispersedly distributed into the mushroom-like 3D hierarchical structure. Fig. 8c and d show the PL excitation and emission spectra of ZnO: Tb^{3+} mushrooms. The excitation spectrum of ZnO: Tb^{3+} mushrooms monitored at 542 nm shows a broad and strong ultraviolet emission at around 408 nm which may be related to oxygen-rich composition, which can be assigned to the electronic transition from the bottom of the conduction band to the V_{Zn} and O_{Zn} defects, respectively.[23,24] The emission spectrum is composed of four well-resolved peaks at 490, 542, 578 and 612 nm, which are attributed to the corresponding characteristic emission $^5D_4 \rightarrow {}^7F_J$ (J = 6, 5, 4, 3) of Tb^{3+} ions.[18] As shown in Fig. 8e and f, both of these luminescent decay curves can be well fit into a single exponential function as $I = I_0 \exp(-t/\tau)$ (where I_0 is the initial intensity at $t = 0$, τ is the 1/e lifetime of the lanthanide ions).[25] According to the fitting results, the lifetime values of ZnO: Eu^{3+} and ZnO: Tb^{3+} mushrooms are determined to be 0.16 and 0.19 ms, respectively.

3. Experimental

All chemicals are of analytical grade reagents and used directly without further purification. $Eu(NO_3)_3$ and $Tb(NO_3)_3$ solutions (0.1 mol/L) were prepared by dissolving the corresponding oxides in diluted nitric acid. Mushroom-like ZnO: Ln^{3+} (Ln = Tb or Eu) was prepared by polyol-mediated method. Firstly, 14.25 mmol of $Zn(CH_3COO)_2{\cdot}2H_2O$ and 9.5 mmol of $(NH_4)_2HPO_4$ were dissolved in 50.0 mL diethylene glycol (DEG), and 2.5 mL of $Eu(NO_3)_3$ or $Tb(NO_3)_3$ solution was added to the above solution under stirring. The mixture was heated under a flow of nitrogen and the temperature of the solution was increased to 160°C under refluxing. After that, the solution was cooled to room temperature and the solid was separated from the solution by centrifugation. In order to remove the residual DEG, the solid was twice resuspended in ethanol and centrifuged again. Finally, the solid was dried at 70 °C for 24 h. In order to investigate the controlled growth of mushroom-like ZnO: Ln^{3+}, the different amounts of $(NH_4)_2HPO_4$ (0, 0.95, 4.75, 19.0, 95.0 mmol) were added to the reaction system, and the other steps were similar to that stated above.

The phase structure of the obtained samples was characterized by a Bruker D8 Advance X-ray diffraction (XRD) with Cu Kα radiation (λ = 0.15406 nm). The accelerating voltage and emission current were 40 kV and 40 mA, respectively. Micrographs were collected using JIB-4501 dual beam with scanning electron microscope (SEM) operating at an acceleration voltage of 30 kV and FEI Quanta 200 SEM, with an acceleration voltage of 25 kV. The scanning transmission electron microscope (STEM) images were obtained by using JEOL-2100F equiped with energy-dispersive X-ray spectroscopy (EDS) with an accelerating voltage of 200 kV. Photoluminescence spectrum and lifetime were recorded by using FLS920P Edinburgh Analytical Instrument apparatus equipped with a 450 W xenon lamp and a μF900H high-energy micro-second flash lamp as the excitation sources. All the measurements were performed at room temperature.

4. Conclusion

In summary, this work has demonstrated a simple and controllable method of synthesizing ZnO: Ln^{3+} mushrooms. The flow of N_2 atmosphere bubbling into the reaction system may play an important role and dramatically affect the phase formation of ZnO. The morphology of ZnO: Ln^{3+} can be evolved from irregular nanoparticles to mushrooms through adjusting the amount of $(NH_4)_2HPO_4$. *I–V* characteristics indicate that ZnO: Ln^{3+} mushrooms exhibit an asymmetrical transport behavior and the anisotropy of electron conductivity. ZnO: Ln^{3+} (Ln = Eu or Tb) samples can exhibit red or green emission under the excitation of UV light. The possible self-assembly mechanism, which is proposed to understand the formation of the ZnO: Ln^{3+} mushrooms, could be applied to build nanoarchitectures with asymmetrical structure and tailor their functionalities. These results open a new way to design and fabricate other mushroom-like 3D hierarchical and asymmetrical structures, which may find new applications in novel optical devices, photonic crystal, biomedicine, catalysis, and so on.

Acknowledgements

This work is financially supported by the National Natural Science Foundation of China (no. 21171179, 21301200,), the Excellent Youth Foundation of He'nan Scientific Committee (no. 134100510018), the Innovation Scientists and Technicians Troop Construction Projects of Henan Province (2013259), and Program for Innovative Research Team (in Science and Technology) in University of Henan Province (no. 14IRTSTHN009).

Notes and references

[a]The Key Laboratory of Rare Earth Functional Materials and Applications, Zhoukou Normal University, Zhoukou 466001, P. R. China
Fax & Tel: +86-394-8178518.
E-mail: zlwang2007@hotmail.com
[b]The College of Chemistry and Molecular Engineering, Zhengzhou University, Zhengzhou 450001, P. R. China
[c]Department of Applied Physics and Materials Research Center, The Hong Kong Polytechnic University, Hong Kong, P. R. China
E-mail: jh.hao@polyu.edu.hk

†Electronic Supplementary Information (ESI) available: [STEM-SEI image and EDS elemental mapping of an individual ZnO: Eu^{3+} mushroom.] See DOI: 10.1039/b000000x/

‡ *These authors have contributed equally.*

1 (a) P. X. Gao, Z. L. Wang, *J. Am. Chem. Soc.* 2003, **125**, 11299; (b) J. Liu, P. X. Gao, W. J. Mai, C. S. Lao, Z. L.Wang, R. Tummala, *Appl. Phys. Lett.* 2006, **89**, 063125; (c) F. R. Fan, Y. Ding, D. Y. Liu, Z. Q. Tian, Z. L. Wang, *J. Am. Chem. Soc.* 2009, **131**, 12036; (d) P. Jiang, J. J. Zhou, H. F. Fang, C. Y. Wang, Z. L. Wang, S. S. Xie, *Adv. Funct. Mater.* 2007, **17**, 1303; (e) P. Yang, X. Xiao, Y. Li, Y. Ding, P. Qiang, X. Tan, W. Mai, Z. Lin, W. Wu, T. Li, *ACS nano* 2013, **7**, 2617.

2 (a) H. M. Xiong, Y. Xu, Q. G. Ren, Y. Y. Xia, *J. Am. Chem. Soc.* 2008, **130**, 7522; (b) S. Xu, Y. Qin, C. Xu, Y. G. Wei, R. S. Yang, Z. L. Wang, *Nat. Nanotechnol.* 2010, **5**, 366; (c) K.-H. Kim, B. Kumar, K. Y. Lee, H.-K. Park, J.-H. Lee, H. H. Lee, H. Jun, D. Lee, S.-W. Kim, *Scientific Reports* 2013, **3**, 2017; (d) M. K. Gupta, J.-H Lee, K. Y. Lee, S.-W. Kim, *ACS Nano* 2013, **7**, 8932; (e) B. Kumar, K. Y. Lee, H.-K. Park, S. J. Chae, Y. H. Lee, S.-W. Kim, *ACS Nano* 2011, **5**, 4197.

3 (a) Y. Ding, P. X. Gao, Z. L. Wang, *J. Am. Chem. Soc.* 2004, **126**, 2066; (b) P. X. Gao, Y. Ding, W. J. Mai, W. L. Hughes, C. S. Lao, Z. L. Wang, *Science* 2005, **309**, 1700; (c) J. Zhou, N. S. Xu, Z. L. Wang, *Adv. Mater.* 2006, **18**, 2432.

4 (a) P. X. Gao, J. H. Song, J. Liu, Z. L. Wang, *Adv. Mater.* 2007, **19**, 67;(b) J. H. Song, Y. Zhang, C. Xu, W. Z. Wu, Z. L. Wang, *Nano Lett.* 2011, **11**, 2829; (c) X. Wu, P. Jiang, Y. Ding, W. Cai, S. S. Xie, Z. L. Wang, *Adv. Mater.* 2007, **19**, 2319; (d) P. Hu, X. Zhang, N. Han, W. Xiang, Y. Cao, F. Yuan, *Cryst. Growth Des.* 2011, **11**, 1520.

5 (a) X. Y. Kong, Z. L. Wang, *Nano Lett.* **2003**, **3**, 1625; (b) P. X. Gao, Z. L. Wang, *Small* 2005, **1**, 945.

6 F. Li, Y. Ding, P. X. Gao, X. Q. Xin, Z. L. Wang, *Angew. Chem. Int. Ed.* 2004, **43**, 5238.

7 S. Xu, Y. Shen, Y. Ding, Z. L. Wang, *Adv. Funct. Mater.* 2010, **20**, 1493.

8 F. H. Zhao, J. G. Zheng, X. F. Yang, X. Y. Li, J. Wang, F. L. Zhao, K. S. Wong, C. L. Liang, M. M. Wu, *Nanoscale* 2010, **2**, 1674.

9 F. Li, F. L. Gong, Y. H. Xiao, A. Q. Zhang, J. H. Zhao, S. M. Fang, D. Z. Jia, *ACS Nano* 2013, **7**, 10482.

10 (a) H. H. Wang, C. S. Xie, D. W. Zeng, Z. H. Yang, *J. Colloid Interface Sci.* 2006, **297**, 570; (b) H. X. Niu, Q. Yang, F. Yu, K. B. Tang, Y. Xie, *Mater. Lett.* 2007, **61**, 137; (c) S. Singh, K. C. Barick, D. Bahadur, *CrystEngComm* 2013, **15**, 4631; (d) X. Wu, B. X. Jia, F. Y. Qu, Q. Q. Zhao, *Curr. Nanosci.* 2014, **10**, 308.

11 (a) X. Li, L. Zhang, Y. Wang, X. Yang, N. Zhao, X. Zhang, J. Xu, *J. Am. Chem. Soc.* 2011, **133**, 3736; (b) T. Tanaka, M. Okayama, Y. Kitayama, Y. Kagawa, M. Okubo, *Langmuir* 2010, **26**, 7843.

12 J. Bae, J. B. Han, X.-M. Zhang, M. Wei, X. Duan, Y. Zhang, Z. L. Wang, *J. Phys. Chem. C* 2009, **113**, 10379.

13 C. Feldmann, *Adv. Funct. Mater.* 2003, **13**, 101.

14 Y. Wang, Y. Zheng, C. Z. Huang, Y. Xia, *J. Am. Chem. Soc.* 2013, **135**, 1941.

15 Z. L. Wang, Z. W. Quan, P. Y. Jia, C. Lin, Y. Luo, Y. Chen, J. Fang, W. Zhou, C. O'Connor, J. Lin, *Chem. Mater.* 2006, **18**, 2030.

16 H. R. Wenk, P. Van. Houtte. *Rep. Prog. Phys.* 2004, **67**, 1367.

17 (a) M. Hossain, A. Mamun, J. Hahn, *J. Phys. Chem. C 2012*, *116*, 23153; (b) C. C. Lin, Y. Y. Li, *Mater. Chem. Phys.* 2009, **113**, 334.

18 D. Yue, W. Lu, C. Y. Li, X. L. Zhang, C. X. Liu, Z. L. Wang, *Nanoscale* 2014, **6**, 2137.

19 H. R. Wenk, P. Van. Houtte. *Rep. Prog. Phys.* 2004, **67**, 1367.

20 D. T. Tu, Y. S. Liu, H. M. Zhu, R. F. Li, L. Q. Liu, X. Y. Chen, *Angew. Chem. Int. Ed.* 2013, **52**, 1128.

21 (a) Y. P. Du, Y. W. Zhang, L. D. Sun, C. H. Yan, *J. Phys. Chem. C* 2008, **112**, 12234; (b) Z. L. Wang, M. Li, C. Wang, J. Z. Chang, H. Z. Shi, J. Lin, *J. Rare Earth* 2009, **27**, 33.

22 (a) Y. H. Wang, Y. S. Liu, Q. B. Xiao, H. M. Zhu, R. F. Li, X. Y. Chen, *Nanoscale* 2011, **3**, 3164; (b) Y. S. Liu, W. Q. Luo, R. F. Li, X. Y. Chen, *Opt. Lett.* 2007, **32**, 566; Y. S. Liu, W. Q. Luo, R. F. Li, G. K. Liu, M. R. Antonio, X. Y. Chen, *J. Phys. Chem. C* 2008, **112**, 686.

23 F. Ochanda, K. Cho, D. Andala, T. C. Keane, A. Atkinson, W. E. Jones Jr, *Langmuir* 2009, **25**, 7547.

24 B. Cheng, Y. Xiao, G. Wu, L. Zhang, *Adv. Funct. Mater.* 2004, **14**, 913.

25 Z. L. Wang, X. L. Zhang, J. Z. Chang, C. Y. Li, *J. Rare Earth* 2011, **29**, 1018.